Engineering Geology 307 (2022) 106790

Contents lists available at ScienceDirect

Engineering Geology

journal homepage: www.elsevier.com/locate/enggeo

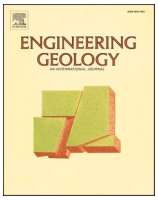

4D electrical resistivity tomography for assessing the influence of vegetation and subsurface moisture on railway cutting condition

Jessica Holmes [a,b,*,1], Jonathan Chambers [b], Paul Wilkinson [b], Ben Dashwood [b], David Gunn [b], Mihai Cimpoiaşu [b], Matthew Kirkham [b], Sebastian Uhlemann [c], Philip Meldrum [b], Oliver Kuras [b], David Huntley [d], Simon Abbott [e], Vinayagamoothy Sivakumar [f], Shane Donohue [g]

[a] Newcastle University, Newcastle, United Kingdom
[b] British Geological Survey, Nottinghamshire, United Kingdom
[c] Lawrence Berkeley National Laboratory, California, United States of America
[d] Geological Survey of Canada, Vancouver, British Columbia, Canada
[e] Network Rail, London, United Kingdom
[f] Queen's University Belfast, Belfast, United Kingdom
[g] University College Dublin, Dublin, Ireland

ARTICLE INFO

Keywords:
Slope stability
Electrical resistivity tomography
Geophysical monitoring
Hydrogeophysics

ABSTRACT

Instability of slopes, embankments, and cuttings on the railway network is increasingly prevalent globally. Monitoring vulnerable infrastructure aids in geotechnical asset management, and improvements to transport safety and efficiency. Here, we examine the use of a novel, near-real-time Electrical Resistivity Tomography (ERT) monitoring system for assessing the stability of a railway cutting in Leicestershire, United Kingdom. In 2015, an ERT monitoring system was installed across a relict landslide (grassed) and an area of more stable ground on either side (wooded), to monitor changes in electrical resistivity through time and space, and to assess the influence of different types of vegetation on the stability of transportation infrastructure. Two years of 4-Dimensional ERT monitoring results are presented here, and petrophysical relationships developed in the laboratory are applied to calibrate the resistivity models in order to provide an insight into hydrogeological pathways within a railway cutting. The influence of vegetation type on subsurface moisture pathways and on slope stability is also assessed – here we find that seasonal subsurface changes in moisture content and soil suction are exacerbated by the presence of trees (wooded area). This results in shrink-swell behaviour of the clays comprising the railway cutting, resulting in fissuring and a reduction in shear strength, leading to instability. As such, it is proposed that on slopes comprised of expansive soils, grassed slopes are beneficial for stability. Insights into the use of 4-D ERT for monitoring railway infrastructure gained from this study may be applied to the monitoring of critical geotechnical assets elsewhere.

1. Introduction

Landslides affecting transport infrastructure are becoming increasingly prevalent (e.g., Jaiswal and van Westen, 2013; Vranken et al., 2013; Simeoni et al., 2014; Vereskun and Yavna, 2015; Laimer, 2017; Liu et al., 2017). In part this is due to age related deterioration of geotechnical assets, many of which are operating well beyond the limit of their design life (Briggs et al., 2019). For example, in the United Kingdom, significant elements of the canal and rail networks were constructed in the 1700s and 1800s and were often poorly engineered (e.g., Gunn et al., 2016), and are therefore displaying particularly poor condition. Moreover, landslide frequency and slope instability is predicted to increase further as the effects of climate change become more prevalent (IPCC, 2014), and in response to changing land use and land cover (Winter et al., 2010; Meneses et al., 2019). Recent effects of changing precipitation patterns have highlighted the vulnerability of transport infrastructure slopes to climatic variations, with numerous failures and major disruption to critical infrastructure (Crozier, 2010).

* Corresponding author at: Newcastle University, Newcastle, United Kingdom.
E-mail address: jessica.holmes@newcastle.ac.uk (J. Holmes).
[1] Previously Queen's University Belfast, Belfast, United Kingdom

https://doi.org/10.1016/j.enggeo.2022.106790
Received 22 March 2022; Received in revised form 13 July 2022; Accepted 14 July 2022
Available online 18 July 2022

Issues associated with aging assets and climate impacts are being exacerbated by increasing urbanization and hence increasing traffic (Hugenschmidt, 2010). As such, there are rising pressures placed on transport networks, and in an age where the transport network is operating at maximum capacity in many places, slope failures on these networks have the potential to result in considerable negative economic, social, and environmental impacts.

Indeed, between 2014 and 2018, there were 381 earthworks failures on assets managed by Network Rail, in addition to 290 temporary speed restrictions relating to asset condition (Network Rail, 2018). Social implications of disruption to transport infrastructure also arise due to delays to travel (Jaroszweski et al., 2014). This highlights a need for monitoring and management of both natural and man-made slopes that affect infrastructure in order to mitigate against such failures.

Traditionally, transport infrastructure slopes are monitored using walkover inspections, to visually identify surface expressions of failure, such as tension cracks (Gunn et al., 2016; Power et al., 2016; Smethurst et al., 2017). In the UK, Network Rail uses risk-based prioritization in the management of approximately 200,000 earthwork assets, combining the likelihood of failure for a particular slope (based upon visual observations) with the likely consequence of failure in a particular location, in order to target and prioritize management (Power et al., 2016). However, vegetation on the surface of the slopes can obscure signs of weakness, and slopes often fail rapidly without precursor signs of instability developing on the slope surface. Discrete point geotechnical surveys are often used in earthworks monitoring to complement visual surveys, but they provide detail about only a small volume of the subsurface. This is problematic as earthwork cuttings and embankments, in particular those built during the industrial revolution, are often highly heterogeneous. As such, discrete point sampling cannot capture the complexity of the subsurface in earthworks assets, which is required if accurate slope stability assessments are to be made (Gunn et al., 2016). In addition, soil sampling disturbance can lead to poor estimates of material properties.

A recent major UK review of railway earthworks management (Mair et al., 2021) identifies key themes and recommendations for improving the serviceability of the transport network and mitigating slope failure. One such recommendation refers to a need to assess the condition of earthworks assets and to identify changes in the subsurface, with a focus on novel technologies. Geophysical techniques present an opportunity to do this, providing detailed subsurface information about large volumes of earthwork structures, and reducing the need for invasive geotechnical investigation. The Network Rail (2018) also recommends a move to remote failure detection. Geophysical surveys have been widely used to monitor subsurface parameters that indirectly influence slope stability (e.g., Bichler et al., 2004; Agnesi et al., 2005; Bruckl et al., 2006; Hibert et al., 2012; Springman et al., 2013; Merritt et al., 2014; Uhlemann et al., 2016; Whiteley et al., 2019). However, whilst there have been some studies focussed on monitoring slopes which affect transport infrastructure using geophysics (e.g., Proto et al., 2010; Donohue et al., 2011; Chambers et al., 2014; Bergamo et al., 2016a, 2016b; Gunn et al., 2018; Holmes et al., 2020; Holmes et al., 2022), this body of research is comparatively small, although it is rapidly expanding.

Electrical Resistivity Tomography (ERT) can be used to monitor earthworks structures and is particularly useful in this context as electrical resistivity is sensitive to spatial variations in lithology so complex subsurface structures of heterogeneous earthworks slopes can be assessed. Additionally, electrical resistivity varies according to moisture content (Waxman and Smits, 1968) and, by extension, soil suction (a factor important in the assessment of slope stability), resistivity of the pore fluid (Archie, 1942), and temperature (Hayley et al., 2007), so changes in these parameters can also be assessed through time and space.

Here, we investigate the use of long-term near-real-time geophysical monitoring of an unstable railway cutting in Old Dalby, Leicestershire, United Kingdom. An ERT monitoring system, PRIME (Proactive Infrastructure Monitoring and Evaluation) (Holmes et al., 2020), is used to provide insight into the changing hydrogeological conditions of the slope with seasonal changes in weather conditions. Petrophysical relationships between electrical resistivity, moisture content, and soil suction were developed in the laboratory and applied to the electrical resistivity models produced from the PRIME monitoring, with the aim of providing direct insights into changes in these parameters through time and space. Specifically, this study aims to investigate the influence of different types of vegetation on subsurface changes in moisture content and soil suction – two factors important in governing the stability of transport infrastructure – through the long-term monitoring of a grassed area and a wooded area of a railway cutting.

2. Study area – the Old Dalby railway test track

The Old Dalby test track is a railway track in Leicestershire, United Kingdom (Fig. 1), which closed to passenger trains in 1967 and to goods trains in 1968. It is now used for the testing of new train designs (Clark, 2004). The Old Dalby Railway test track includes sections of cut slopes, which have a history of instability. The studied section of the Old Dalby railway cutting was selected for this research owing to its history of instability – the grassed area in the centre of the slope is the site of a relict landslide. On either side of this landslide, the railway cutting is wooded, with broadleaf deciduous trees, predominantly Hawthorne. This spatial variation in vegetation cover enabled a comparison of the influence of vegetation type on subsurface resistivity.

The study site is located in a temperate climatic zone, and weather patterns vary seasonally. Summers tend to be warm and dry, and winters are cold and wet. The average annual temperature in Leicestershire, where the Old Dalby railway cutting is located, is 9.9 °C, with the highest and lowest monthly average temperatures of 16.7 °C and 4.2 °C in July and January respectively (Climate-Data.org, 2022). Average precipitation is 707 mm per year (ibid.).

A borehole core was taken from the top of the slope of the Old Dalby railway cutting, the location of which is shown in Fig. 2. The core taken provides lithostratigraphic information on the upper 6.83 m of the Old Dalby cutting. Percussion drilling was used to obtain the core, using a 102 mm barrel with 1 m of casing. At 4 m depth, the barrel size was reduced to 87 mm to aid progression. Non-contact resistivity imaging was used to log the core, without disturbing the material (Jackson et al., 2006). This meant that core material could also be used to develop petrophysical relationships, as described later in this paper. To make the measurements, the core was placed on a table over a transmitter coil that produced a primary magnetic field that induced electric currents in the sample. The induced currents produce a secondary magnetic field that is inversely proportional to the resistivity of the core. Resistivity was also measured using galvanic current, by inserting potential electrodes along the length of the core and introducing current at each end of the core. Similar results were obtained from both measurement methods, indicating the validity of the results. Material taken from the core was also used to establish the particle size distribution of the material from the Old Dalby cutting.

The borehole core taken from the Old Dalby site demonstrates the main geology at the site. Fig. 3 shows the core alongside the resistivity logs. The lowermost unit identified in this core, which ranges from 6.0 to 6.83 m below the surface, is identified as the Blue Anchor Formation, and has a lower resistivity than the upper 6.0 m of the core. The Blue Anchor Formation is composed of pale green-grey siltstone and mudstone and was deposited in mixed continental and marine waters (Ambrose, 1998).

Overlying the Blue Anchor formation in parts of the site is the Westbury Formation, which formed as part of the Penarth Group during a marine transgression (Ambrose, 1998; Carney et al., 2004), and is comprised of fissile mudstones and thin sandstone. However, this formation is poorly exposed as it is highly susceptible to weathering (Carney et al., 2004). The material comprising the Old Dalby railway

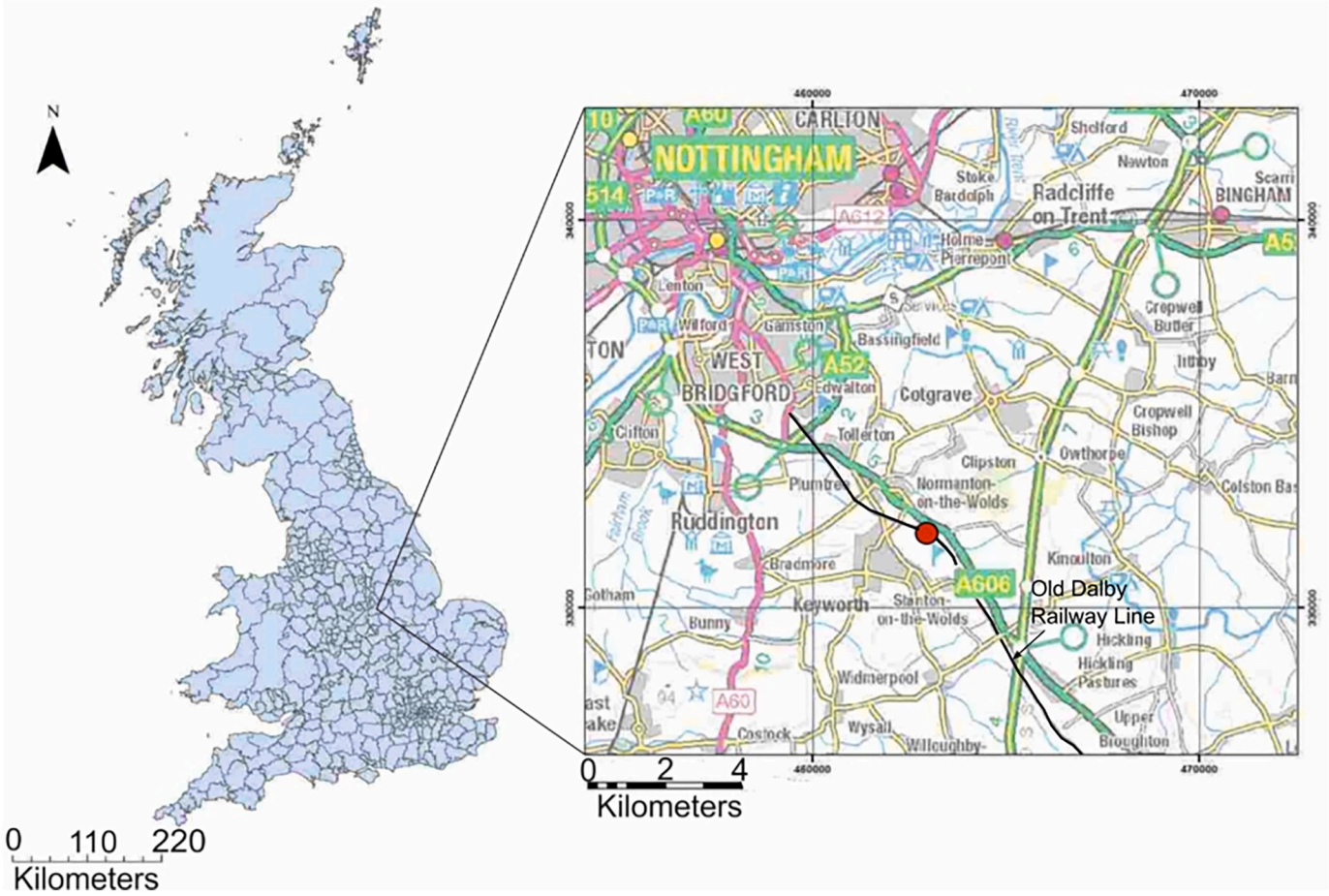

Fig. 1. Location of the Old Dalby test track, Leicestershire, UK. The location of the railway cutting monitored in this study is shown by the red marker. (For interpretation of the references to colour in this figure legend, the reader is referred to the web version of this article.)

cutting and represented in the core is a Quaternary glacial till called the Thrussington Till, from approximately 0.7 to 6.0 m depth. The Thrussington Till is comprised of a stiff fine-grained, red-brown matrix with occasion gravel inclusions (derived from local Penarth and Mercia rocks). Topsoil makes up the uppermost 0.7 m of the core.

A 3-D ground model was developed for the Old Dalby railway cutting using borehole data from the top of the PRIME-monitored section of the slope, along with the ERT images produced from the PRIME ERT data, and a Digital Elevation Model of the site. ERT models were imported into Paraview, a data analysis and visualisation application (Ayachit, 2015), and lithological boundaries were identified in the borehole logs from the site. This information, alongside previous geological interpretations from geology maps of the site was used to inform the location of the lithological boundaries across the PRIME-monitored area of the site. One boundary was identified - between Blue Anchor Till and the overlying Thrussington Till – and this boundary was digitized on the model in 3-D. This enabled the visualisation of geological cross-sections along each array line of the ERT model and allowed for the calibration of the model with petrophysical relationships relevant to the specific material properties present in each zone of the slope.

Fig. 4 shows a simple 3-Dimensional ground model of the Old Dalby railway cutting. This reveals horizontal bedding at the site, with Thrussington Till comprising the upper part of the slope, and overlying Blue Anchor Till at the toe of the slope. This ground model was used to determine which of the petrophysical relationships developed in the lab for each material should be used for the calibration of each region of the model. It should be noted here that this simple ground model is based on a single borehole, and then better-defined using resistivity models. As such, there may be variation within the geological setting of the Old Dalby railway cutting that is not captured by this model, which highlights a limitation of the research.

The particle size distribution tests of the Thrussington Till and the Blue Anchor Formation indicate both formations to be a sandy clay (Table 1).

3. Methodology

3.1. Time-lapse ERT monitoring

A near-real-time ERT monitoring system, PRIME (Proactive Infrastructure Monitoring and Evaluation) (Holmes et al., 2020) installed on the Old Dalby railway cutting actively collected data for two years (July 2015 to July 2017). The PRIME installation consisted of multiple electrode arrays connected to the PRIME system, which made electrical resistivity measurements at 12-h intervals and sent the data to a remote server via an internet connection, allowing the site to be repeatedly monitored to develop a 4-D ERT dataset. Buried, stainless steel, rod electrodes were set out in 5 lines, 2 running across slope, and 3 running down slope, as shown in Fig. 2, extending across a relict landslide and sections of un-slipped cutting either side. Lines 1 and 2 consisted of 91 electrodes at 1 m spacing, and Lines 3, 4, and 5 consisted of 19 electrodes at 1 m spacing. The system was powered using a 100 W solar panel, making it independent from mains power supply.

Use of the PRIME system here allowed for automated remote data collection, which eliminated the need for repeat manual ERT surveys. This is an important consideration for transport infrastructure assets as

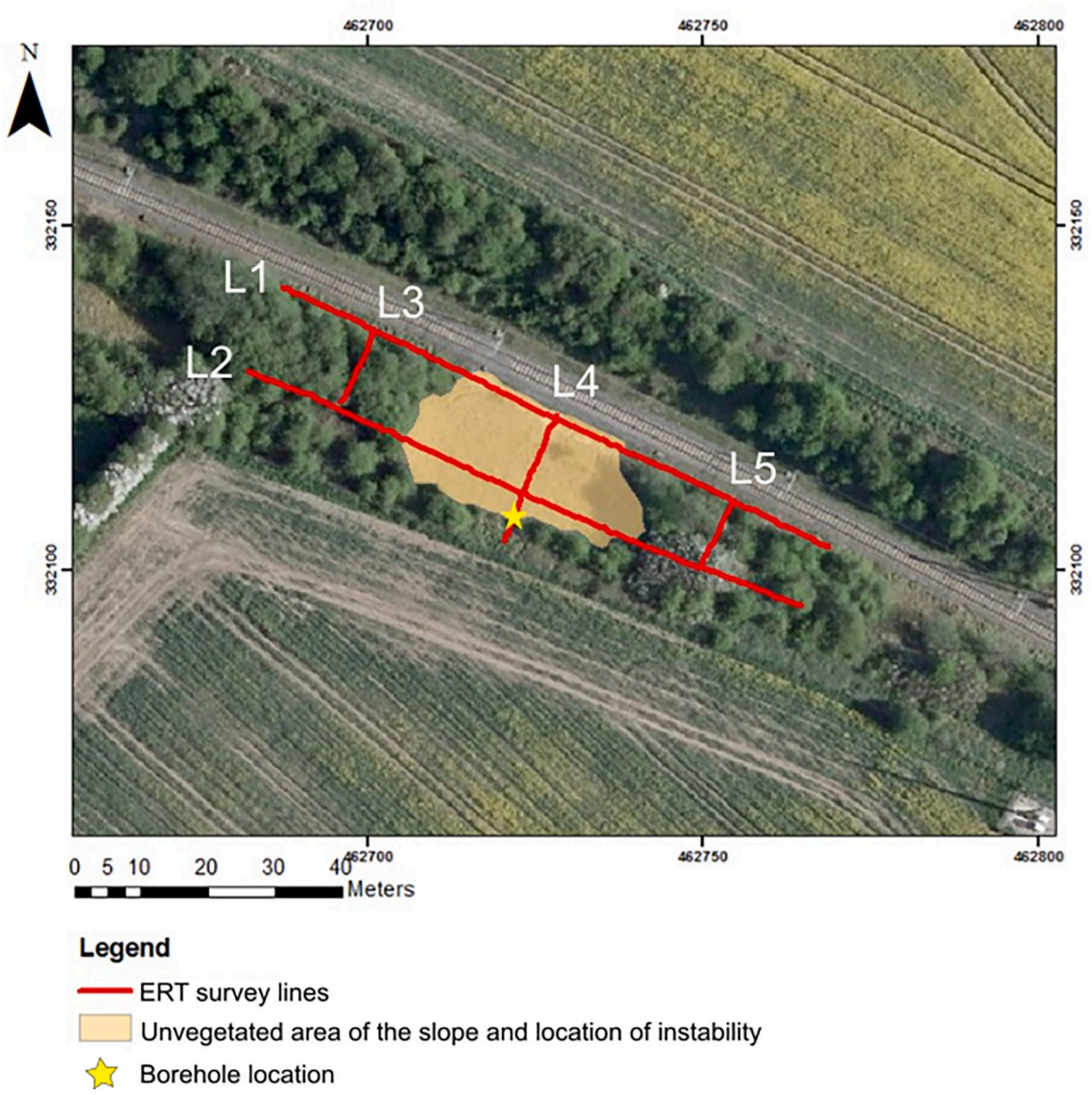

Fig. 2. PRIME installation on the Old Dalby railway cutting, showing location of the ERT arrays, and the vegetated (wooded) and non-vegetated (grassed) areas of the slope. The location of a borehole used to establish the geology of the railway cutting is highlighted by the yellow star. Line numbers (L1 – L5) are also shown. (For interpretation of the references to colour in this figure legend, the reader is referred to the web version of this article.)

active railway lines are hazardous environments. Additionally, the temporal resolution offered by the twice-daily measurement scheme implemented here allows a detailed interpretation of subsurface changes in electrical resistivity in response to changing soil moisture conditions through time and space. As the ERT arrays extend across both wooded and grassed areas of the slope (Fig. 2), an assessment of the importance of vegetation cover on soil moisture dynamics could also be considered.

Resistivity data was filtered to remove any poor-quality measurements; data with high contact resistances (>1 kΩ) or negative transfer resistances were removed from the dataset. Reciprocal errors were calculated using the forward and reciprocal measurements taken by the PRIME system to produce error models for each dataset in the time-lapse inversion (Lesparre et al., 2017). Any measurements with high reciprocal errors (>5%) were filtered out of the dataset to improve the fit of the data to the model during geophysical inversion (Tso et al., 2017).

The resistivity data were inverted using an iteratively reweighted Gauss-Newton least-squared method in Res3DInvx64 from Geotomo Software (Loke et al., 2003; Loke, 2017). To avoid overfitting, the inversion process was stopped once the reduction in absolute misfit between subsequent iterations was <5%. The inversion constraints were selected to ensure the most accurate model possible was obtained: an L2-norm spatial smoothness constraint was selected to provide spatial smoothing. Smoothing was stronger in the horizontal direction than in the vertical direction (2:1), as the predominant change in resistivity occurs parallel to the slope surface (i.e., wetting and drying of the near-surface). Additionally, for each ERT line (Fig. 2), all of the data from each individual time step were combined into a single file and inverted simultaneously using an L1-norm temporal smoothness constraint. Data for each line was inverted in 3-D to account for offline variations in topography and to allow for some resistivity variation in the direction perpendicular to the line (Holmes et al., 2020). The perpendicular extent of the model was half the vertical extent and the discretisation in the off-line direction was twice as coarse, promoting more vertical variation of resistivity while allowing for a degree of off-line variation. The fact that the resistivity of a large volume of the subsurface is modelled using a grid of 5 electrode arrays is a potential limitation of the method, owing to the uncertainty associated with resistivity values for regions of the model that are far from the location of the electrode arrays. As such,the resulting models are displayed using only the cells directly below the electrode lines to display the vertical model variation clearly.

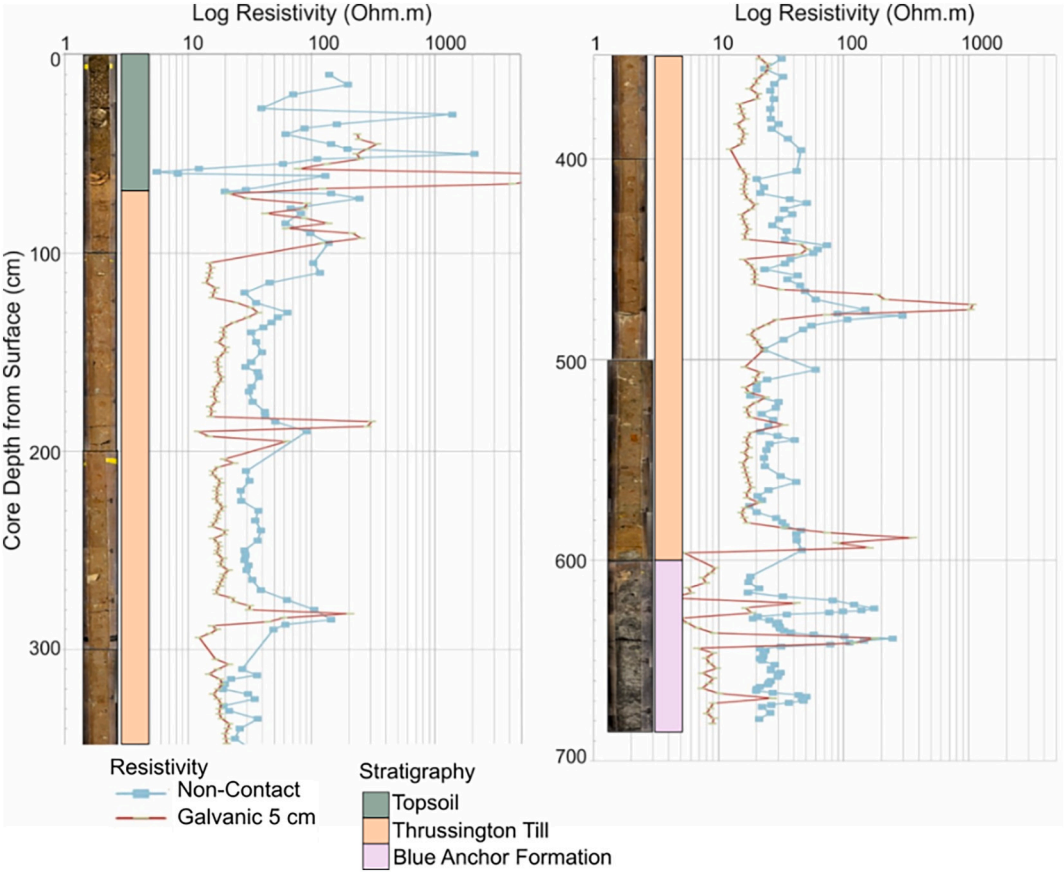

Fig. 3. Borehole log from the Old Dalby railway cutting, with non-contact and galvanic resistivity (Resistivity data from Guérin, 2018).

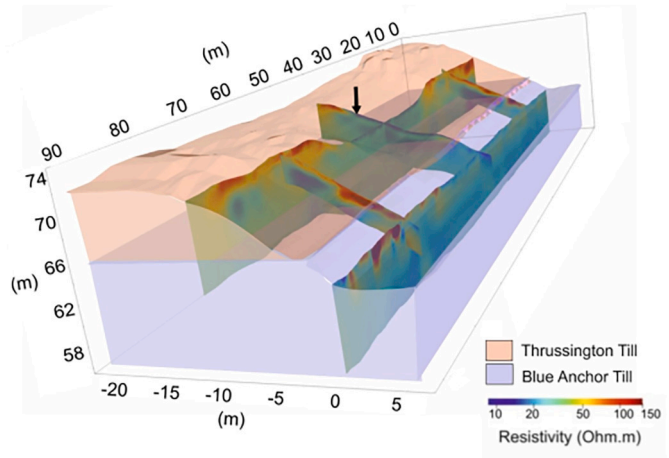

Fig. 4. 3-D ground model of the Old Dalby railway cutting, incorporating baseline ERT models. The black arrow marks the location of the borehole at the site.

3.2. Development of laboratory-based petrophysical relationships

The relationship between electrical resistivity and soil moisture content can be described by petrophysical models such as Waxman and Smits (1968), and Archie's Law (Archie, 1942). Given that moisture content is a key control on slope stability, an understanding of the relationship between moisture content and electrical resistivity is imperative for drawing interpretations from the PRIME models. Soil suction also has a close relationship with soil moisture content. As such, indirect relationships can also be established between soil suction and electrical resistivity (e.g., Merritt et al., 2016; Holmes et al., 2020). Here, relationships between electrical resistivity, moisture content, and soil suction were developed in the laboratory such that the PRIME model images can be discussed in terms of changes in moisture content and soil suction.

Table 1
Particle size distribution of Old Dalby material.

Lithological Unit	Grain Size (%)			
	Clay (<0.0063 mm)	Silt (0.063–0.05 mm	Sand (0.05–2 mm)	Gravel (>2 mm)
Thrussington Till	45.9	19.0	31.5	3.6
Blue Anchor Till	69.0	17.4	13.6	0

3.2.1. Soil matric suction measurements

Here, a Water Potential Meter WP4C (Meter Group) was used to measure matric suction (MPa) to 1% accuracy between −5 and − 300 MPa. Samples (5 mm depth, 37 mm diameter) were cut out following compaction of material taken from Old Dalby at maximum dry density (12.5% moisture content by weight) in a Proctor mould using British Standard methodology (BS1377–4), as in-situ density information was not available due to limited site access. Samples were allowed to dry for set amounts of time (30 min to 2 h) so that suction measurements could be carried out at different moisture contents. During wetting cycles, distilled water was added to the samples using a pipette, and the samples were left to equilibrate for at least 2 h before suction was measured.

3.2.2. Electrical resistivity measurements

Electrical resistivity was also measured in the laboratory at different moisture contents to establish a relationship between resistivity and soil moisture. For the Thrussington Till, this was completed using coffin tests.

Firstly, a Proctor sample was produced at maximum dry density using British Standard methodology. Samples (25 × 25 × 75 mm) were placed in perforated plastic coffins (Fig. 5) for resistivity measurements. Each coffin had a current electrode at either end of the sample, and two potential electrodes in the middle of the sample, spaced 25 mm apart. Resistivity coffin samples were taken from the Proctor mould both horizontally and vertically to determine the effect of anisotropy on resistivity measurements. Measurements were taken at different moisture contents over several wetting and drying cycles.

A function generator with a frequency of 60-Hz was used, and the current was altered throughout the wetting and drying cycles (ranging between 537 and 5664 μA). The injection current was measured across a 20 Ω resistor. The resulting voltage was measured across the two potential electrodes using an oscilloscope.

Firstly, the geometric factor of the sample was calculated:

$$G = \frac{\varnothing}{1000\,X} \tag{1}$$

Where G is the geometric factor, $\varnothing$ is the cross-sectional area of the sample (mm^2), and X is the electrode separation of the potential electrodes (mm).

The oscilloscope readings, along with the known current were then used to calculate the resistance of the sample:

$$R_{soil} = \frac{V_{soil}}{I} \tag{2}$$

Where R_{soil} is the resistance of the sample (Ω), V_{soil} is the voltage across the sample (V) (half the peak to peak voltage measured on the oscilloscope), and I is the applied current (A).

This was then used to calculate the resistivity of the sample, ρ_{soil} (Ωm):

$$\rho_{soil} = R_{soil} G \tag{3}$$

Given that temperature has a considerable influence on geoelectrical measurements, with conductivity increasing linearly with temperature above 0 °C (Hayley et al., 2007), the temperature of the room was also recorded during each measurement, which allowed to correct the resistivity for variations in sample temperature:

$$\rho_T = \rho_{soil}(1 + 0.02(T - 25)) \tag{4}$$

Where ρ_T is temperature-corrected resistivity (Ωm), and T is temperature (°C). Temperature correction was made to 25 °C to enable comparison with other methodologies used here which use an ES-2 sensor where measurements are automatically corrected to 25 °C.

3.2.3. Modified HYPROP2 experiments

Here, a novel methodology for the simultaneous measurement of soil suction and electrical resistivity provides the opportunity to develop direct relationships between suction, resistivity and moisture content (Holmes et al., 2022) for the Blue Anchor Formation from the Old Dalby Railway Cutting. Samples were reconstituted and compacted using British Standard methodology to in-situ dry density. Experiments were attempted for the Thrussington Till, but compaction of the sample resulted in pore water pressure building up at compaction boundaries, making saturation impossible.

Modification of HYPROP 2 equipment (Meter Group) enabled a four-point resistivity array to be inserted into the sample to allow for simultaneous measurements of suction, moisture content, and resistivity, and provided direct relationships between these parameters (See Holmes et al., 2022 for methodological details).

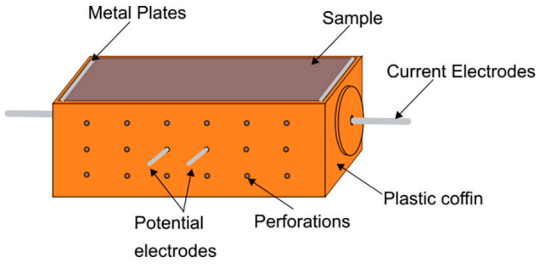

Fig. 5. Coffins used to measure the electrical resistivity of samples.

3.2.4. Calibration of ERT models

A modified Waxman-Smits model was fitted to the resistivity and moisture content data measured in the laboratory, as in Uhlemann et al. (2017):

$$\rho(GMC) = F\left(\frac{(1-\varphi)D_g GMC}{\varphi D_w}\right)^{-n}\left(\sigma_w + B_{ws}\left[\frac{(1-\varphi)D_g C}{100\varphi}\right]\left[\frac{\varphi D_w}{(1-\varphi)D_g GMC}\right]\right)^{-1} \tag{5}$$

Where, F is a formation factor, φ is porosity, D_g is grain density (g cm^{-3}), D_w is water density (g cm^{-3}), n is a saturation exponent, σ_w is the pore water conductivity (S/m), and C is cation exchange capacity (meq/100 g). The average cation mobility, B_{ws} (S cm^3 m^{-1} meq^{-1}), was estimated from the empirical fit given by Waxman and Smits (1968). Each parameter was measured in the laboratory, with the exception of F and n, which were fitted (there is uncertainty in these values as although these values fit the data, they are not unique) and B_{ws}, which was estimated (Waxman and Smits, 1968):

$$\left(B_{ws} = 4.6\left(1 - 0.06\,Exp\left[-\frac{\sigma_w}{1.3}\right]\right)\right. \tag{6}$$

Waxman-Smits models were fitted to the data from each lithological unit tested in the laboratory in order to convert electrical resistivity to gravimetric moisture content. The resulting models were used for the calibration of the ERT models generated from data from the PRIME system. The parameters used in this calculation for each lithological unit are shown in Table 2.

Further utilising the direct relationship between electrical resistivity, moisture content, and matric suction, a relationship between resistivity and soil suction can be established.

Fredlund and Xing (1994) present an equation that relates soil water content (θ) with soil suction (ψ):

$$\theta = \theta_s\left[\frac{1}{ln\left[e + (\psi/a)^t\right]}\right]^b \tag{7}$$

where θ_s is water content at saturation, and a, t, and b are fitting parameters, and e is Euler's number. This can be written in terms of gravimetric moisture content:

$$GMC = \frac{D_w}{D_g}\theta(\psi) = \frac{D_w}{D_g}\theta_s y(\psi)^{-b} \tag{8}$$

where

$$y = ln\left[e + \left(\frac{\psi}{a}\right)^t\right] \tag{9}$$

If we replace GMC in [8] with its expression from [6], it yields a relationship between bulk electrical resistivity and suction:

$$\rho(\psi) = F\left(\frac{(1-\phi)\theta_s y(\psi)^{-b}}{\phi}\right)^{-n}\left(\sigma_w + B_{ws}\left[\frac{(1-\phi)D_g C}{100\phi}\right]\left[\frac{\phi y(\psi)^b}{(1-\phi)\theta_s}\right]\right)^{-1} \tag{10}$$

Eq. 10 and measurements of suction and resistivity on material from the Old Dalby railway cutting were used to fit the model for the

Table 2
Parameters used in the fitting of Waxman-Smits models to laboratory data from the Old Dalby Railway Cutting (Formation factor, *F*, a fitting parameter, *n*, porosity, *Φ*, grain density, D_g, water density, D_w, pore water conductivity, σ_w, average mobility of cations, B_{ws}, and cation exchange capacity, *C)*.

Waxman-Smits Model	F (−)	n (−)	Φ (−)	D_g (g/cm^3)	D_w (g/cm^3)	σ_w (S/m)	B_{ws} (S cm^3 m^{-1} meq^{-1})	C (meq/100 g)
Thrussington Till	7.992	2.244	0.35	2.65	1	0.031	1.91	10.8
Blue Anchor	5.565	2.709	0.49	2.72	1	0.249	2.32	21.9

estimation of soil suction from resistivity for calibration of the PRIME ERT models. Here, this calibration is only made for the Thrussington Till, as this allowed for comparison with soil sensors installed at the site of the Old Dalby railway cutting, located in the Thrussington Till unit. The parameters used in eq. 9 for this calibration are shown in Table 3.

3.3. Field sensor measurements

In addition to the PRIME system at the Old Dalby site, other field sensors were installed to provide further monitoring data to inform interpretations from the PRIME ERT models. An ECRN-100 Rain Gauge (METER Group) was installed at the top of the slope on Line 4 (central line) of the PRIME system. This provided rainfall data for the duration of the PRIME monitoring period. In addition to this, GS3 and 5TE sensors, which monitor soil moisture content, electrical conductivity, and temperature, were installed at 0.15 m depth in the Thrussington Till and at 2.6 m depth in the Blue Anchor, respectively.

Effective rainfall – total rainfall minus evapotranspiration – was calculated, using the rainfall data from the ECRN-100 rain gauge. Here, evapotranspiration was calculated using the Hargreaves-Samani equation (Hargreaves and Samani, 1982; Samani, 2000), which uses temperature (measured on site), and a latitude-based radiation approximation to estimate evapotranspiration:

$$ET = 0.0135(KT)(R_a)(TD)^{1/2}(TC + 17.8) \quad (11)$$

Where *ET* is evapotranspiration, *KT* is an empirical coefficient, R_a is extra-terrestrial radiation, *TD* is temperature difference between the maximum and minimum recorded temperature (°C) ($T_{max} - T_{min}$), and *TC* is the average daily air temperature (°C).

4. Results and discussion

4.1. Petrophysical relationships

Results of the electrical resistivity-moisture content relationship experiments are shown in Fig. 6 for both the Thrussington Till and the Blue Anchor units, and the Waxman-Smits model fitted to each dataset is displayed. There is a clear relationship between electrical resistivity and gravimetric moisture content, with a non-linear decrease in electrical resistivity as soil moisture increases. In the coffin tests, the effect of anisotropy on the resistivity measurements is clear – there is a distinction between measurements made on the vertically cut and horizontally cut coffin samples, where at lower moisture contents, the resistivity of the coffins with vertically cut samples was higher than that of the horizontally cut samples. This phenomenon is observed in the literature: Merritt et al. (2016) stated that in material with high silt and clay contents, measurements taken perpendicular to the bedding planes (vertical coffin tests here) show higher values of resistivity than measurements taken parallel to the bedding planes (horizontal coffin tests here). This shows a clear anisotropy in the measurements owing to preferential current flow along bedding planes (Merritt et al., 2016) and highlights a source of potential error and uncertainty in making interpretations of moisture content based on electrical resistivity. Here, an average of the vertical and horizontal measurements was taken and used for the development of a Waxman-Smits relationship for calibration of the field ERT models.

Table 3
Parameters used for the fitting of a suction-GMC model.

Suction-GMC Model	a (kPa)	n (−)	b (−)	t (−)
Thrussington Till	817.16	2.24	13.51	0.13

There is uncertainty in these values as although these values fit the data, they are not unique.

These relationships were used for the calibration of the ERT models to provide a direct interpretation of the changes in moisture content and soil suction through space and time, as opposed to inferring moisture content changes from changes in resistivity.

Fig. 7 shows the relationship between soil suction (negative pore water pressure) and moisture content for the Thrussington Till. Again, there is a non-linear relationship between these two parameters; suction increases exponentially with decreasing moisture content, and the correlation within each wetting and drying cycle has an R^2 value of over 0.95 in all cases. As soil suction is clearly related to moisture content, and resistivity is also closely correlated to moisture content, it is also possible to infer changes in matric suction from changes in electrical resistivity.

4.2. 4-dimensional electrical resistivity tomography

A temperature-corrected baseline ERT image from the PRIME monitoring (05/05/2016) at the Old Dalby test track is shown in Fig. 8. The wooded areas of the slope captured by the monitoring on Line 3 and Line 5, and the areas of Lines 1 and 2 that intercept them, exhibit higher baseline values of electrical resistivity. Line 4, and the areas of Lines 1 and 2 that it intercepts, have lower baseline values of resistivity, and are grassed. This contrast in resistivity is due to the impact of soil moisture variations, as wooded areas of the slope are dryer than grassed areas due to root uptake of soil moisture during the summer months. Also present in Line 1 is a counterfort drain, shown by a high resistivity zone surrounded by a lower resistivity zone caused by preferential movement of groundwater in the soil in this area. This image was selected as the baseline as it is midway between the maximum resistivity values in summer and the minimum resistivity values in winter.

The ERT models were calibrated using the laboratory-developed petrophysical relationships shown in Fig. 6, with different relationships applied to different zones of the model according to the 3-D ground model (Fig. 4). Fig. 9 shows the baseline image of the ERT models (Fig. 8) converted to show the spatial distribution of gravimetric moisture content (GMC). Fig. 10 shows the percentage change in GMC through time and space, showing percentage change from this calibrated baseline image. Positive changes in GMC are indicative of wetting, and negative changes in GMC are indicative of drying. Two years of PRIME monitoring data from Old Dalby are presented in Fig. 10. Changes in GMC over this period are shown through bimonthly snapshots of the Old Dalby railway cutting from July 2015 to June 2017.

Fig. 10 shows a clear preferential wetting at the toe of the Old Dalby railway cutting, characterised here by an increase in GMC from the spring baseline. This occurs in the region of the counterfort drain, identified in Fig. 8. The increase in moisture content observed here has implications for soil suction (negative pore water pressure), which is important for slope stability as if soil suction is decreased sufficiently it can induce slope failure (Fredlund et al., 1978). Indeed, tension cracks

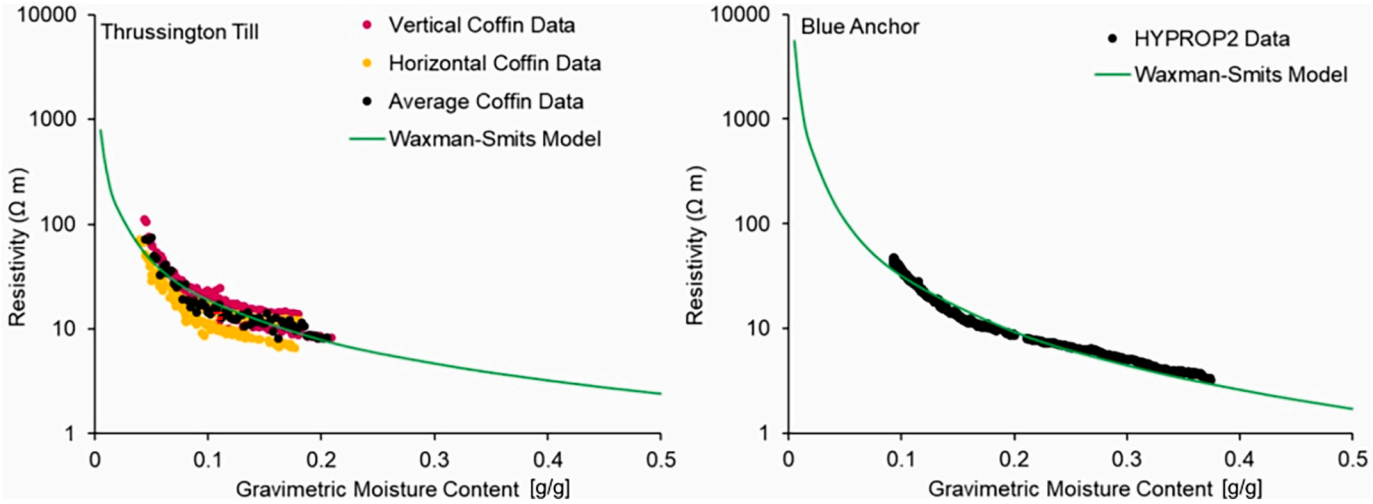

Fig. 6. Relationship between gravimetric moisture content and electrical resistivity for the Thrussington Till and the Blue Anchor Formation, with Waxman-Smits models fitted. (For interpretation of the references to colour in this figure legend, the reader is referred to the web version of this article.)

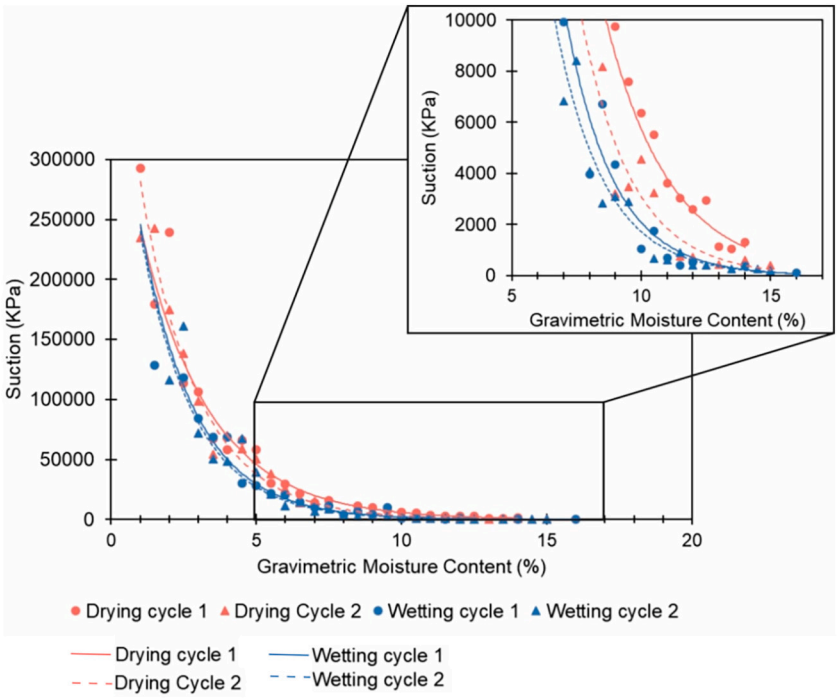

Fig. 7. Relationship between soil suction and gravimetric water content based on WP4C suction measurements carried out in the laboratory for the Thrussington Till.

are observed at the surface in this region, indicating early signs of instability.

Most notably at the site of the Old Dalby railway cutting, the changes in resistivity, and therefore in soil moisture content, are exacerbated by the presence of vegetation, as shown by the spatial disparities in resistivity in Fig. 8, Fig. 9, and Fig. 10. The wooded regions of the slope (predominantly on Lines 3 and 5 (Fig. 2)) undergo much greater changes in resistivity (and, therefore, in GMC) seasonally than the grassed regions. The wooded areas of the slope have a low resistivity during winter months and high resistivity during summer months, with an average high resistivity of 50.9 Ω m in summer, and an average low resistivity of 26.0 Ω m in winter. Conversely, the grassed area of the slope (around Line 4 (Fig. 2)) undergoes little change between summer and winter, with a small resistivity range of 20.4–25.3 Ω m across the monitoring period.

This effect is also clear in Fig. 11, which shows GMC (converted from resistivity) through time for wooded and grassed regions of the monitored volume of the slope. To differentiate between wooded and grassed areas of the model, a mask was applied to the model data that isolated the cells of the model in the wooded and grassed zones respectively, and then the average GMC of these cells was calculated for each time step in the model. The average GMC is shown for the entire depth of the ERT models. Effective rainfall data is also shown alongside this, such that interpretations of changes in resistivity in response to soil moisture variation can be informed by knowledge of weather conditions.

Data from the moisture content sensors (GS3 and 5TE) installed on the slope are also shown in Fig. 11. In summer months, high values of electrical resistivity in wooded areas correspond to low volumetric moisture content during periods of negative effective rainfall, as evidenced by field sensor data (Fig. 11). In winter, lower values of electrical

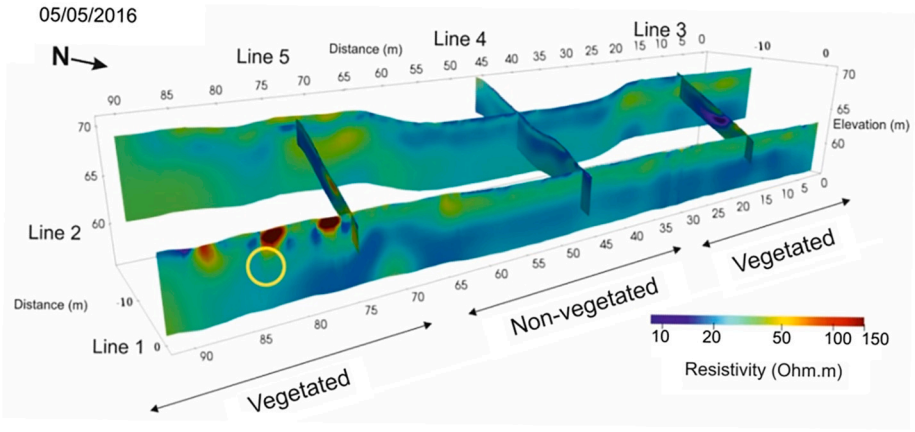

Fig. 8. Baseline image from the PRIME electrical resistivity monitoring at the Old Dalby railway cutting, from 05/05/2016. Wooded and grassed regions of the model are highlighted. The yellow ring highlights the location of a counterfort drain in the railway cutting. (For interpretation of the references to colour in this figure legend, the reader is referred to the web version of this article.)

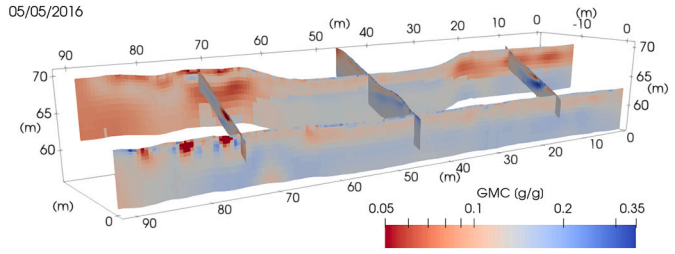

Fig. 9. Baseline image from the PRIME electrical resistivity monitoring at the Old Dalby railway cutting, from 05/05/2016, converted using petrophysical relationships to display spatial variation in gravimetric moisture content.

resistivity in the wooded areas of the slope correspond to higher volumetric moisture content in the subsurface, which occurs in response to positive effective rainfall. The changes in moisture content at 0.15 m below the surface correspond closely to the changes in rainfall over short time-periods, but the moisture content at 2.6 m depth relates to seasonal changes in soil moisture content. Indeed, the moisture content rises sharply at 2.6 m depth following prolonged rainfall in winter, coinciding with reduced resistivity in the subsurface and falls during dry periods when effective rainfall is negative during the summer, coinciding with an increase in average resistivity in the subsurface (Fig. 10).

However, the seasonal changes in resistivity observed in the wooded areas are not seen in the grassed areas of the slope (Fig. 10 and Fig. 11). The role of vegetation in controlling spatial distributions of soil moisture is greater during the summer due to increased plant activity as a result of higher air temperatures and longer daylight hours, causing higher rates of photosynthesis, plant growth, transpiration, and root water uptake (Rodríguez-Iturbe and Porporato, 2004; Vivoni et al., 2008). In winter, plant activity is reduced, which explains the reduction in the difference in resistivity between wooded and grassed areas during this time. Additionally, tree-covered ground is likely to be drier in summer due to interception of rainfall and the canopy storage function of broadleaf species, and the difference between the moisture content of the wooded and grassed areas is diminished during winter owing to leaf loss.

The disparity in the extent to which changes in soil moisture content are exacerbated by plant activity is strongly dependent on the type of vegetation: Grass has a longer growing season than trees, particularly during early spring, prior to the emergence of leaves on broadleaf trees (Harding et al., 1992). This effect can be seen in Fig. 10 where there is an increase in GMC across the wooded area in response to positive effective rainfall in the image from 03/03/2017 and 24/03/2017, but very little change in the grassed area owing to root uptake of water. Therefore, there is a spatial disparity in seasonal responses to changing weather conditions owing to the vegetation type.

Owing to the associated controls on soil moisture, as is indicated by the changes in electrical resistivity observed here, the type of vegetation cover on slopes is an important consideration for the assessment of the integrity and stability of transport infrastructure assets. In wooded areas, the GMC ranged between 0.095 and 0.130 g/g, whereas for grass, the range was much narrower, ranging between 0.124 and 0.138 g/g. While the presence of roots can increase slope stability due to increased cohesion, repeated wetting and drying cycles can result in volumetric deformation with shrink-swell behaviour, and a reduction in shear strength (Khan et al., 2019). Previous studies report similar findings: for example, vertical displacement of a railway embankment comprising London Clay fill was an order of magnitude greater adjacent to a tree-covered area, when compared with a grass-covered area (Scott, 2006). Indeed, near to the Old Dalby PRIME installation, surface signs of slope instability are observed in the wooded zone, with tension cracks appearing. This highlights the need to consider vegetation in the assessment of slope stability on the transport network. Due to the shrink-swell behaviour associated with trees and the high levels of soil moisture associated with grasses, a combination of vegetation types is suggested.

While the presence of trees can increase slope stability due to increased cohesion and reduced surface erosion from roots, it is also noted that in sites where the slip plane of the landslide occurs below the root level, additional weight from trees can increase displacement (Ziemer, 1981). As such, where slopes are already unstable, unlike the Old Dalby railway cutting, tree felling is recommended to mitigate this effect. However, in clay soils removal of trees can result in a temporary increase in suction, leading to softening as a result of moisture migration to the felled area (Greenwood et al., 2004). As such, careful consideration of the geological setting of an embankment or cutting must be made in order for mitigation of slope instability to be effective.

Changes in soil suction through time at the Old Dalby Railway Cutting are shown in Fig. 12. The resistivity of the cells in the ERT models proximal to the location of moisture content sensors in the field was averaged for each time step, and the models shown in Fig. 7 were applied to provide changes in suction through time. Field measurements of GMC are shown alongside this. As expected, as GMC increased, soil suction decreased, as there is a monotonic relationship between moisture content and soil suction. Soil suction is lowest during the winter when plant activity is at a minimum, and gradually increases in line with the seasonal decrease in GMC due to evapotranspiration and increased root uptake of soil moisture in the summer months and associated drying of the slope in the wooded areas. This data further highlights the cyclic changes in subsurface conditions that are known to induce shrink-swell

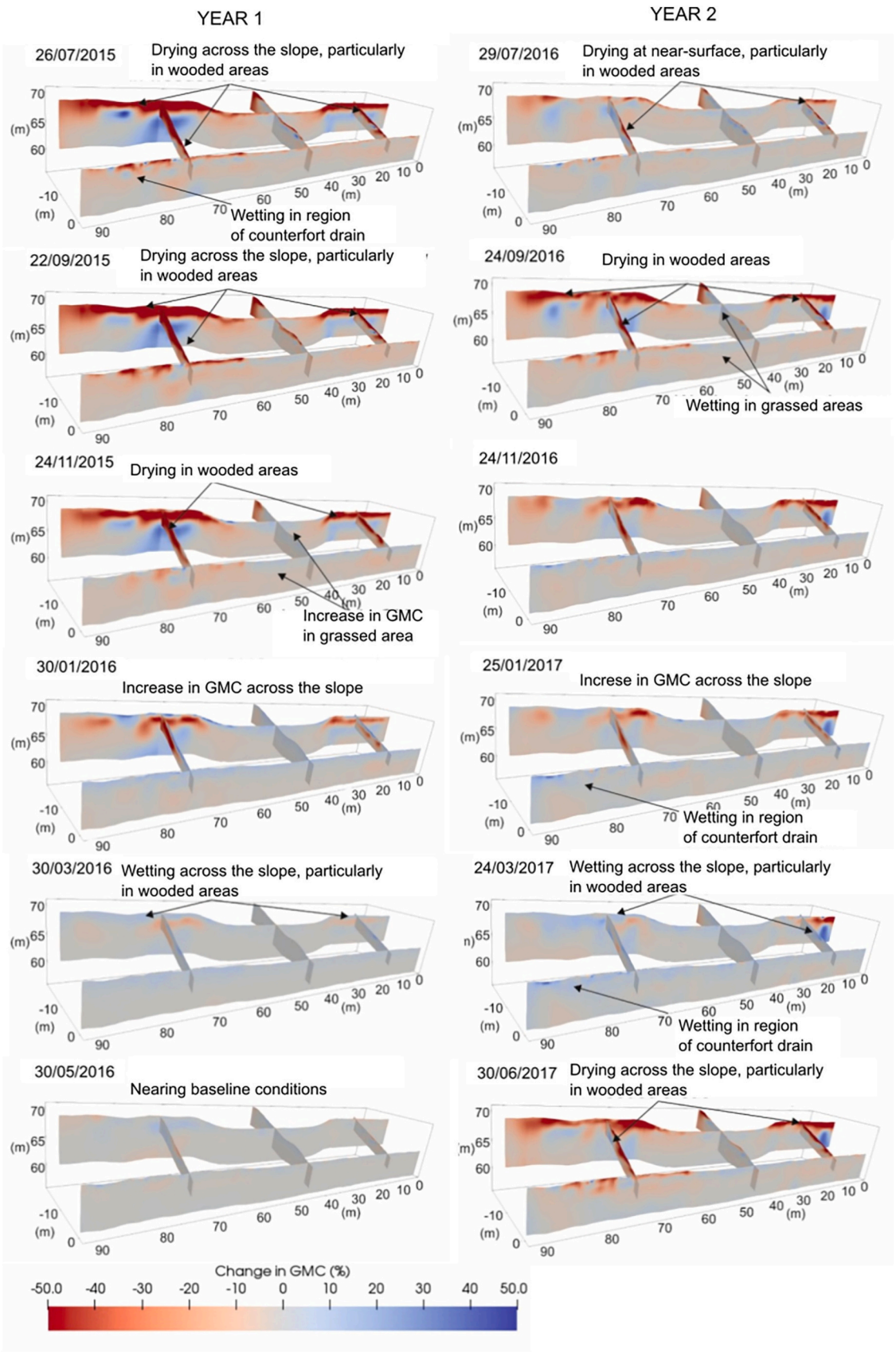

Fig. 10. Percentage change in gravimetric moisture content on the Old Dalby railway cutting from a baseline level (05/05/2016) through the 2-year monitoring period.

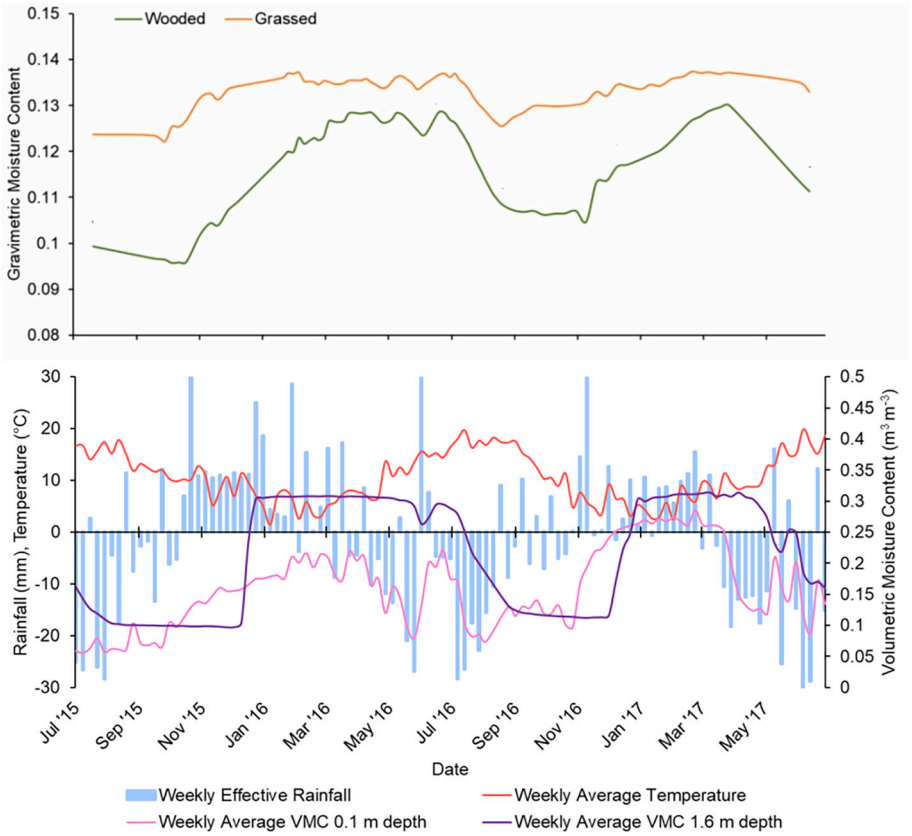

Fig. 11. Weather data from Old Dalby field sensors, including rainfall data, temperature data and ground volumetric moisture content (VMC) data from 0.15 m depth and 2.6 m depth. This is shown beneath average gravimetric moisture content (GMC) for the vegetated (wooded) and non-vegetated (grassed) areas of the slope.

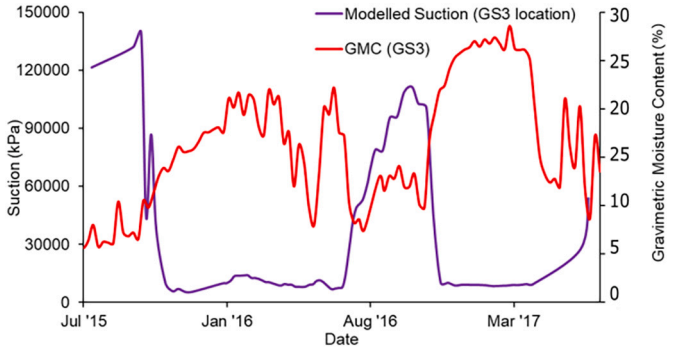

Fig. 12. Suction modelled using laboratory-based petrophysical relationship and measured gravimetric moisture content at the Old Dalby Railway Cutting.

related deterioration of slope material, eventually leading weakening and failure.

5. Conclusions

The subsurface response to seasonal changes in weather conditions at the Old Dalby railway cutting has been assessed through 4-D ground imaging using a PRIME (Proactive Infrastructure Monitoring and Evaluation) system installed at the site. 4-D geoelectrical monitoring at Old Dalby reveals a clear hydrogeological regime that responds closely to changes in surface weather conditions on a seasonal basis, with surface drying during summer months, and wetting of the subsurface during winter months. Most notable here is the spatial disparity in the seasonal response to changing weather conditions. The resistivity of the grassed area of the slope was not observed to change significantly over time, whereas the resistivity of wooded areas was much higher in summer than in winter, responding more closely to changes in effective rainfall. This is due to greater plant activity during summer (transpiration, root water uptake, accelerated growth, and photosynthesis), which results in greater drying at the surface of wooded zones compared to grassed zones. This highlights the utility of geoelectrical monitoring for monitoring transport infrastructure slopes, as it provides insight into moisture pathways and spatial heterogeneities that cannot be identified using traditional asset monitoring techniques. Therefore, given that many asset stability issues are related to high moisture content, ERT is a useful tool in asset monitoring as it provides an effective means of imaging drainage processes. Additionally, the need to consider vegetation in the assessment of slope stability on the transport network has been highlighted: while trees can improve cohesion of soils on transport infrastructure assets, the increased seasonal changes in moisture content owing to the presence of trees can increase shrink-swell behaviour, leading to slope destabilisation. As such, trees are not recommended for planting on slopes comprised of expansive soils proximal to transport infrastructure. This study shows that non-invasive, automated, remote ERT monitoring can be an effective tool in imaging such processes, highlighting its use as a monitoring tool for infrastructure assets.

CRediT authorship contribution statement

Jessica Holmes: Conceptualization, Methodology, Investigation, Writing – original draft, Writing – review & editing, Visualization, Formal analysis. **Jonathan Chambers:** Conceptualization, Supervision, Methodology, Writing – review & editing. **Paul Wilkinson:** Conceptualization, Supervision, Software, Formal analysis, Writing – review & editing. **Ben Dashwood:** Methodology. **David Gunn:** Methodology. **Mihai Cimpoiaşu:** Formal analysis, Writing – review & editing. **Matthew Kirkham:** Resources. **Sebastian Uhlemann:** Conceptualization, Formal

analysis. **Philip Meldrum:** Methodology, Software. **Oliver Kuras:** Conceptualization. **David Huntley:** Supervision. **Simon Abbott:** Resources. **Vinayagamoothy Sivakumar:** Supervision. **Shane Donohue:** Conceptualization, Supervision, Methodology, Writing – review & editing.

Declaration of Competing Interest

The authors declare that they have no known competing financial interests or personal relationships that could have appeared to influence the work reported in this paper.

Data availability

Data will be made available on request.

Acknowledgments

This research is a collaborative effort between several research institutions (Queen's University Belfast, the British Geological Survey (BGS), Lawrence Berkeley National Laboratory, The Geological Survey of Canada, and University College Dublin). The authors wish to thank Network Rail for facilitating the research. Holmes, Chambers, Wilkinson, Dashwood, Gunn, Cimpoias¸u, Kirkham, Meldrum, and Kuras publish with permission of the Executive Director of the BGS (UKRI). The first author was funded by the Department for the Economy, Northern Ireland and the British Geological Survey. The BGS contribution is linked to the ACHILLES project (EPSRC grant reference EP/R034575/1). The contribution of Uhlemann was supported by the Laboratory Directed Research and Development Program of Lawrence Berkeley National Laboratory under U.S. Department of Energy Contract No. DEAC02- 05CH11231. The last author's contribution is funded with the financial support of Science Foundation Ireland, Geological Survey of Ireland and the Environmental Protection Agency under the SFI Frontiers for the Future Programme 19/FFP/6535.

References

Agnesi, V., Camarda, M., Conoscenti, C., Di Maggio, C., Diliberto, I.S., Madonia, P., Rotigliano, E., 2005. A multidisciplinary approach to the evaluation of the mechanism that triggered the Cerda landslide (Sicily, Italy). Geomorphology 65, 101–116.

Ambrose, K., 1998. Geology of the Old Dalby area. British Geological Survey. Technical Report WM98/16.

Archie, G.E., 1942. The electrical resistivity log as an aid in determining some reservoir characteristics. Trans. Am. Inst. Min. Metall. Pet. Eng. 146, 54–62.

Ayachit, U., 2015. The ParaView Guide: A Parallel Visualization Application. Kitware. ISBN 978-1930934306.

Bergamo, P., Dashwood, B., Uhlemann, S., Swift, R., Chambers, J.E., Gunn, D.A., Donohue, S., 2016a. Time-lapse monitoring of climate effects on earthworks using surface waves. Geophysics 81 (2), EN1–EN15.

Bergamo, P., Dashwood, B., Uhlemann, S., Swift, R., Chambers, J.E., Gunn, D.A., Donohue, S., 2016b. Time-lapse monitoring of fluid-induced geophysical property variations within an unstable earthwork using P-wave refraction. Geophysics 81 (4), EN17–EN27.

Bichler, A., Bobrowsky, P., Best, M., Douma, M., Hunter, J., Calvert, T., Burns, R., 2004. Three-dimensional mapping of a landslide using a multi-geophysical approach: the Quesnel Forks landslide. Landslides 1, 29–40.

Briggs, K.M., Dijkstra, T.A., Glendinning, S., DeJong, M.J., Schooling, J.M., Viggiani, G. M.B., 2019. Evaluating the deterioration of geotechnical infrastructure assets using performance curves. In: International Conference on Smart Infrastructure and Construction, 2019. https://doi.org/10.1680/icsic.64669.429.

Bruckl, E., Brunner, F.K., Kraus, K., 2006. Kinematics of a deep-seated landslide derived from photogrammetric, GPS and geophysical data. Eng. Geol. 88, 149–159.

Carney, J.N., Ambrose, K., Brandon, A., Lewis, M.A., Royles, C.P., Sheppard, T.H., 2004. Geology of the Country around Melton Mowbray. Sheet description of the British Geological Survey, 1:50 000 Series. Sheet 142 (England and Wales).

Chambers, J.E., Gunn, D.A., Wilkinson, P.B., Meldrum, P.I., Haslam, E., Holyoake, S., Kirkham, M., Juras, O., Merritt, A., Wragg, J., 2014. 4D electrical resistivity tomography monitoring of soil moisture dynamics in an operational railway embankment. Near Surf. Geophys. 12, 61–72.

Clark, R., 2004. Rail flaw detection: overview and needs for future developments. NDT & E International 37, 111–118.

Climate-Data.org, 2022. Climate Leicester (United Kingdom). https://en.climate-data.org/europe/united-kingdom/england/leicester-17/ [Accessed: 28/06/2022].

Crozier, M.J., 2010. Deciphering the effect of climate change on landslide activity: a review. Geomorphology. 124 (3–4), 260–267.

Donohue, S., Gavin, K., Tolooiyan, A., 2011. Geophysical and geotechnical assessment of a railway embankment failure. Near Surf. Geophys. 9 (1), 33–44.

Fredlund, D.G., Xing, A., 1994. Equations for the soil-water characteristic curve. Can. Geotech. J. 31, 521–532.

Fredlund, D.G., Morgenstern, N.R., Widger, R.A., 1978. The shear strength of unsaturated soil. Can. Geotech. J. 15, 313–321.

Greenwood, J.R., Norris, J.E., Wint, J., 2004. Assessing the contribution of vegetation to slope stability. Proceedings of the Institution of Civil Engineers - Geotechnical Engineering 157 (4), 199–207, 2004.

Guérin, A., 2018. The Old Dalby Landslide: Rock Physics and Electrical Resistivity Tomography Monitoring. Masters Thesis. University of Liège, Belgium.

Gunn, D., Dashwood, B.A.J., Bergamo, P., Donohue, S., 2016. Aged embankment imaging and assessment using surface waves. Forensic Engineering. Proc. Inst. Civ. Eng. 169 (4), 149–165.

Gunn, D.A., Chambers, J.E., Dashwood, B.E., Lacinska, A., Dijkstra, T., Uhlemann, S., Swift, R., Kirkham, M., Milodowski, A., Wragg, J., Donohue, S., 2018. Deterioration model and condition monitoring of aged railway embankment using non-invasive geophysics. Constr. Build. Mater. 170, 668–678.

Harding, R.J., Hall, R.L., Neal, C., Roberts, J.M., Rosier, P.T.W., Kinniburgh, D.G., 1992. Hydrological impacts of broadleaf woodlands: Implications for water use and water quality. Institute of Hydrology, British Geological Survey Project Report 115/03/ST for the National Rivers Authority. Institute of Hydrology, Wallingford.

Hargreaves, G.H., Samani, Z.A., 1982. Estimating potential evapotranspiration. J. Irrig. and Drain Engr., ASCE 108 (IR3), 223–230.

Hayley, K., Bentley, L.R., Gharibi, M., Nightingale, M., 2007. Low temperature dependence of electrical resistivity: implications for near surface geophysical monitoring. Geophys. Res. Lett. 34 (18).

Hibert, C., Grandjean, G., Bitri, A., Travelletti, J., Malet, J.P., 2012. Characterizing landslides through geophysical data fusion: example of the La Valette landslide (France). Eng. Geol. 128, 23–29.

Holmes, J., Chambers, J., Meldrum, P., Wilkinson, P., Boyd, J., Williamson, P., Huntley, D., Sattler, K., Elwood, D., Sivakumar, V., Reeves, H., Donohue, S., 2020. 4-Dimensional Electrical Resistivity Tomography for continuous, near-real time monitoring of a landslide affecting transport infrastructure in British Columbia, Canada. Near Surf. Geophys. 18 (4).

Holmes, J., Chambers, J., Wilkinson, P., Meldrum, P., Cimpoiaşu, M., Boyd, J., Huntley, D., Williamson, P., Gunn, D., Dashwood, B., Whiteley, J., Watlet, A., Kirkham, M., Sattler, K., Elwood, D., Sivakumar, V., Donohue, S., 2022. Application of petrophysical relationships to electrical resistivity models for assessing the stability of a landslide in British Columbia, Canada. Eng. Geol. 301, 106613.

Hugenschmidt, J., 2010. Geophysics and non-destructive testing for transport infrastructure, with special emphasis on ground penetrating radar. PhD thesis. ETH Zurich.

IPCC, 2014. Climate Change 2014: Synthesis Report. Contribution of Working Groups I, II and III to the Fifth Assessment Report of the Intergovernmental Panel on Climate Change [Core Writing Team, R.K. Pachauri and L.A. Meyer (Eds.)]. IPCC, Geneva, Switzerland, 151 pp.

Jackson, P.D., Lovell, M., Roberts, J.A., Schultheiss, P., Gunn, D.A., Flint, R.C., Wood, A., Holmes, R., Frederichs, T., 2006. Rapid non-contacting resistivity logging of core. Geol. Soc. Lond., Spec. Publ. 267 https://doi.org/10.1144/GSL.SP.2006.267.01.15.

Jaiswal, P., Van Westen, C.J., 2013. Use of quantitative landslide hazard and risk information for local disaster risk reduction along a transportation corridor: a case study from Nilgiri district, India. Nat. Hazards 65, 887–913.

Jaroszweski, D., Hooper, E., Baker, C., Chapman, L., Quinn, A., 2014. The impacts of the 28 June 2012 storms on UK road and rail transport. Meteorol. Appl. 22 (3), 470–476.

Khan, S., Ivoke, J., Nobahar, M., 2019. Coupled effect of wet-dry cycles and rainfall on highway slope made of Yazoo Clay. Geosciences 9, 341.

Laimer, H.J., 2017. Anthropogenically induced landslides - a challenge for railway infrastructure in mountainous regions. Eng. Geol. 222, 92–101.

Lesparre, N., Nguyen, F., Kemna, A., Robert, T., Hermans, T., Daoudi, Flores-Orozco, A., 2017. A new approach for time-lapse data weighting in electrical resistivity tomography. Geophysics 82, E325–E333.

Liu, J.X., Yang, C.H., Gan, J.J., Liu, Y.T., Wei, L., Xie, Q., 2017. Stability analysis of road embankment slope subjected to rainfall considering runoff-unsaturated seepage and unsaturated fluid-solid coupling. Int. J. Civ. Eng. 15, 865–876.

Loke, M.H., 2017. RES3DINVx64 ver. 4.07 with multi-core and 64-bit support for Windows XP/Vista/7/8/10. Rapid 3-D Resistivity & IP inversion using the least-squares method. Geoelectrical Imaging 2-D and 3-D. Geotomo Software.

Loke, M.H., Acworth, I., Dahlin, T., 2003. A comparison of smooth and blocky inversion methods in 2D electrical imaging surveys. Explor. Geophys. 34, 182–187.

Mair, R., Hight, D., McGinnity, B., 2021. A Review of Earthworks Management. Network Rail 543.

Meneses, B.M., Pereira, S., Reis, E., 2019. Effects of different land use and land cover data on the landslide susceptibility zonation of road networks. Nat. Hazards Earth Syst. Sci. 19, 471–487.

Merritt, A.J., Chambers, J.E., Murphy, W., Wilkinson, P.B., West, L.J., Gunn, D.A., Meldrum, P.I., Kirkham, M., Dixon, N., 2014. 3D ground model development for an active landslide in Lias mudrocks using geophysical, remote sensing and geotechnical methods. Landslides. 11 (4), 537–550.

Merritt, A.J., Chambers, J.E., Wilkinson, P.B., West, L.J., Murphy, W., Gunn, D., Uhlemann, S., 2016. Measurement and modelling of moisture – electrical resistivity relationship of fine-grained unsaturated soils and electrical anisotropy. J. Appl. Geophys. 124, 155–165. https://doi.org/10.1016/j.jappgeo.2015.11.005.

Network Rail, 2018. Earthworks Technical Strategy. June 2018, p. 67.
Network Rail, 2018. Network Rail Earthworks Technical Strategy. June 2018 [Available at: https://www.networkrail.co.uk/wpcontent/uploads/2018/07/Earthworks-Technical-Strategy.pdf].
Power, C., Mian, J., Spink, T., Abbott, S., Edwards, M., 2016. Development of an Evidence-based Geotechnical Asset Management Policy for Network Rail, Great Britain. Procedia Engineering, 143, pp. 726–733.
Proto, M., Bavusi, M., Bernini, R., Bigagli, L., Bost, M., Bourquin, F., Cottineau, L.-M., Cuomo, V., Vecchia, P.D., Dolce, M., Dumoulin, J., Eppelbaum, L., Fornaro, G., Gustafsson, M., Hugenschmidt, J., Kapersen, P., Kim, H., Lapenna, V., Leggio, M., Loperte, A., Mazzetti, P., Claudio, M., Nativi, S., Nordebo, S., Pacini, F., Palombo, A., Pascucci, S., Perrone, A., Pignatti, S., Ponzo, F.C., Rizzo, E., Soldovieri, F., Taillade, F., 2010. Transport infrastructure surveillence and monitoring by electromagnetic sensing: the ISTIMES project. Sensors. 10 (12), 10620–10639.
Rodríguez-Iturbe, I., Porporato, A., 2004. Ecohydrology of Water-Controlled Ecosystems: Soil Moisture and Plant Dynamics. Cambridge Press, Cambridge, p. 422.
Samani, Z., 2000. Estimating solar radiation and evapotranspiration using minimum climatological data. J. Irrig. Drain. Eng. 126 (4), 265–267.
Scott, J.M., 2006. Influence of vegetation on the performance of railway embankments. In: Szavits-Nossan, V. (Ed.), Proceedings of the 17th European, Young Geotechnical Engineers Conference, Zagreb, 2006. Croatian Geotechnical Society, Velika Gorica, Croatia, pp. 101–112.
Simeoni, L., Ronchetti, F., Corsini, A., Mongiovi, L., 2014. Interaction of Extremely Slow Landslides with Transport Structures in the Alpine Glacial Isarco Valley.X11 IAEG Congress, Turin. 14th September. https://doi.org/10.1007/978-3-319-09057-3_37.
Smethurst, J.A., Smith, A., Uhlemann, S., Wooff, C., Chambers, J., Hughes, P., Lenart, S., Saroglou, H., Springman, S.M., Löfroth, Hughes, D., 2017. Current and future role of instrumentation and monitoring in the performance of transport infrastructure slopes. Quart. J. Eng. Geol Hyrdogeol. 50, 271–286.
Springman, S.M., Thielen, A., Kienzler, P., Friedel, S., 2013. A long-term field study for the investigation of rainfall-induced landslides. Geotechnique 63, 1177–1193.
Tso, C.H.M., Kuras, O., Wilkinson, P.B., Uhlemann, S., Chambers, J.E., Meldrum, P.I., Graham, J., Sherlock, E.F., Binley, A., 2017. Improved characterisation and modelling of measurement errors in electrical resistivity tomography (ERT) surveys. J. Appl. Geophys. 146, 103–119.
Uhlemann, S., Smith, A., Chambers, J.E., Dixon, N., Dijkstra, T., Haslam, T., Meldrum, P., Merritt, A., Gunn, D., Mackay, J., 2016. Assessment of ground-based monitoring techniques applied to landslide investigation. Geomorphology. https://doi.org/10.1016/j.geomorph.2015.10.027.
Uhlemann, S., Chambers, J., Wilkinson, P., Maurer, H., Merritt, A., Meldrum, P., Kuras, O., Gunn, D., Smith, A., Dijkstra, T., 2017. Four-dimensional imaging of moisture dynamics during landslide reactivation. J. Geophys. Res. Earth Surf. 122 (1), 398–418.
Vereskun, V.D., Yavna, V.A., 2015. Geotechnical methods of reinforcement of slopes near railroads. Sci. Cold Arid Regions 7, 469–474.
Vivoni, E.R., Rinehart, A.J., Méndez-Barroso, L.A., Aragón, C.A., Bisht, G., Cardenas, M. B., Engle, E., Forman, B.A., Frisbee, M.D., Gutiérrez-Jurado, H.A., Hong, S., Mahmood, T.H., Tai, K., Wyckoff, R.L., 2008. Vegetation controls on soil moisture distribution in the Valles Caldera, New Mexico, during the North American monsoon. Ecohydrology 1, 225–238. https://doi.org/10.1002/eco.11.
Vranken, L., Van Turnhout, P., Vas Den Eeckhaut, M., Vandekerckhove, L., Poesen, J., 2013. Economic valuation of landslide damage in hilly regions: a case study from Flanders, Belgium. Sci. Total Environ. 447, 323–336.
Waxman, M.H., Smits, L.J.M., 1968. Electrical conductivities in oil-bearing shaly sands. Soc. Pet. Eng. J. 8, 107–122.
Whiteley, J., Chambers, J., Uhlemann, S., Wilkinson, P., Kendall, J., 2019. Geophysical monitoring of moisture-induced landslides: a review. Rev. Geophys. 57 (1), 106–145.
Winter, M.G., Dixon, N., Wasowski, J., Dijkstra, T.A., 2010. Introduction to land-use and climate change impacts on landslides. Q. J. Eng. Geol. Hydrogeol. 43, 367–370.
Ziemer, R.R., 1981. The Role of Vegetation in the Stability of Forested Slopes. Proceedings of the International Union of Forestry Research Organizations, XVII World Congress, 6–2017 September 198l. Kyoto, Japan, vol. I, pp. 297–308.